

Structural behavior of CFRP strengthened concrete-filled steel tubes columns under axial compression loads

Jai Woo Park¹ and Sung Mo Choi^{*2}

¹Gayoon Construction Co., Ltd., Seoul, Korea

²The University of Seoul, Department of Architecture Engineering, Seoul, Korea

(Received June 05, 2012, Revised March 25, 2013, Accepted April 22, 2013)

Abstract. This paper presents the structural behavior of CFRP (carbon fiber reinforced polymer) strengthened CFT (concrete-filled steel tubes) columns under axial loads. Circular and square specimens were selected to investigate the retrofitting effects of CFRP sheet on CFT columns. Test parameters are cross section of CFT, D/t (B/t) ratios, and the number of CFRP layers. The load and ductility capacities were evaluated for each specimen. Structural behavior comparisons of circular and rectangular section will be represented in the experimental result discussion section. Finally, ultimate load formula of CFRP strengthened CFT will be proposed to calculate the ultimate strength of CFRP strengthened circular CFT. The prediction values are in good agreement with the test results obtained in this study and in the literature.

Keywords: concrete-filled steel tubes (CFT); composite column; confinement effect; carbon fiber sheet; FRP

1. Introduction

1.1 Backgrounds

Fiber reinforced polymers (FRPs) have been widely used for structure strengthening applications during the past 25 years in the construction fields. FRPs have high tensile strength, high corrosion resistance, and ease-hand construction workability. However, the most common application was used in RC structures and most researches have focused in RC strengthening methods. The FRPs are embedded into or externally attached to RC members to improve confinement, flexural strength, shear strength and fatigue life.

Recently, with the solution of many of the practical and theoretical problems for FRP/RC technology, some researchers have started to focus on the use of FRP to strengthen steel members. Carbon fiber reinforced polymer (CFRP) is externally attached to the bottom flanges of steel or composite girder to increase flexural capacity (Miller *et al* 2001, Schnerch *et al.* 2007, 2008, Fam *et al.* 2009, Sallam *et al.* 2010). El-Tawil *et al.* (2011) studied the enhancing stability of steel columns with FRP strips. CFRP was used to enhance the plastic hinge region of double-channel members of chord members of a special truss moment frame. From the test, the CFRP could

*Corresponding author, Professor, E-mail: smc@uos.ac.kr

inhibit the local buckling of the channel flanges. Finally, it was concluded that the improved ductility of the plastic hinge region was achieved as compared to unreinforced specimens. Teng *et al.* (2007) conducted a structural test for FRP strengthened short hollow section steel columns. They found that for short columns, transverse CFRP layers are effective in confining the outward local buckling. Bambach *et al.* (2009) conducted an experimental study for axial capacity and design of thin-walled steel SHS strengthened with CFRP. Harries *et al.* (2009) conducted an experimental test on enhancing stability of structural steel sections using FRP strips. By applying FRP materials, the steel compression member could have the improved global and local buckling behavior. Narmashiri *et al.* (2010) conducted a structural test on shear strengthening method of steel I beams by CFRP strips. 5 specimens were fabricated to investigate the effectiveness of shear strengthening of steel I-beams by using CFRP strips on the shear zone. The CFRP strips were attached on both or one side of steel I-beam web. From the test, it was concluded that CFRP strip shear methods of steel I-beams web were a successful method for increasing load capacity and decreasing deformation of structural members.

1.2 FRP strengthened CFT columns

In the recent year, CFT column have widely been used in columns of tall-buildings and bridge piers. The composites column can combine the advantages of steel and concrete. CFT columns can provide not only an increase in the load carrying and ductility capacity but also rapid construction and construction cost saving. However, CFT columns have the disadvantage that is local buckling after steel tube yielding and deterioration in concrete's confinement effect causing failure. To solve the problem, Xiao *et al.* (2005) proposed the new CFT column system (CCFT), where CFRP sheet were used as additional confinement material to inhibit potential plastic hinge regions of the columns. Axial load tests were conducted with 13 specimens. Test result showed that CFRP strengthened circular CFT columns showed a bi-linear load-displacement curve similar to CFRP confined concrete. The load capacity was improved up to 54~136% compared with the existing CFT columns. Xiao *et al.* (2005) also conducted an experimental test on FRP confined circular CFT columns under axial and cyclic loads. The CFRP sheet was attached at the end of the columns, which is the potential plastic hinge zone. Test result showed that because the CFRP sheet could delay the local buckling of the steel tubes, the ductility capacities of the CFRP strengthened CFT columns were increased and the CFRP confinement could provide to improve seismic performance. Tao *et al.* (2007a) conducted a study on CFRP strengthened circular and square CFT columns under axial loads. 9 specimens were fabricated. Test results contained the load and ductility capacities of each section of CFT under the effect of CFRP wraps. He also proposed an axial design formula of CFRP strengthened circular CFT columns. Tao *et al.* (2007b) also conducted axial load test on CFRP strengthened CFT after exposure to fire. From the test, fire-damaged CFT columns can be restored by CFRP retrofitting. Park *et al.* (2010) conducted the seismic tests of CFRP strengthened square CFT columns. Test results showed that the ductility capacities of CFRP strengthened CFT were clearly increased compared with those of the un-strengthened CFT. Therefore, it was concluded that CFRP confinement could provide improvement of seismic performance.

1.3 Research objectives

This study aims at observing the behavior of FRP strengthened CFT columns under axial loads

and at verifying the CFRP retrofitting effect. Both circular and square CFT columns were prepared. The main parameters are the number of FRP layers and D/t (B/t) ratio. 19 specimens were prepared and the axial loading test was conducted. Also, a simplified equation will be proposed to calculate the ultimate strength of FRP strengthened circular CFT columns.

2. Test plans and failure procedure of specimens

2.1 Specimen plans

19 specimens were fabricated according to the test variable plan for central axial load tests in order to observe the axial behavior of CFT columns confined by both carbon fiber sheets (CFRP sheets) and steel. Among the 19 specimens, 10 were circular and 9 were square. Test parameters were sectional shape (circular and square), diameter-thickness ratio (D/t) or width-thickness ratio (B/t) and the number of CFRP layers. AISC provision (2005) specifies the limit for the width to thickness ratio (B/t) of steel hollow square section and the diameter to thickness ratio (D/t) of steel hollow circular section, respectively.

The diameter and length of CFT circular specimens were 139.8 mm and 620 mm, respectively. The thickness of steel tubes was 3.2 mm, 4.5 mm and 6.6 mm. Diameter-thickness ratio (D/t) ranged between 21 and 44. The number of CFRP sheet layers on steel tubes was 0, 1 and 3 ply. One circular specimen strengthened with 2 layers of CFRP sheets was also fabricated to observe the behavior different from those reinforced with 1 and 3 layers. Design compressive strength of the concrete inside the steel tubes was 36 MPa.

The sectional width and length of CFT square specimens were 125 mm and 550 mm, respectively. The thickness of steel tubes was 3.0 mm, 4.5 mm and 6.0 mm and width-thickness ratio (B/t) ranged between 21 and 39. The number of CFRP sheet layers was 0, 1 and 3 ply. The design compressive strength of concrete was 50MPa. Fig. 1 and Table 1 are specimen details and test variables.

2.2 Material tests

The design compressive strength of the concrete filled in steel tubes was 36 MPa for circular CFT columns and 50 MPa for square columns and the result from the 28-day-test was 37.5, 49MPa, respectively. The yield strength of 3.2 mm, 4.5 mm and 6.2 mm-thick circular specimens was 365 MPa, 334 MPa and 301 MPa, respectively. The yield strength of 3.0 mm, 4.5 mm and 6.0mm-thick square specimens was 304 MPa, 300 MPa and 324 MPa, respectively. The thickness and tensile strength of carbon fiber sheets provided by the FRP manufacturer were 0.111 mm/ply and 3,500 MPa, respectively.

2.3 Test setup

Fig. 2 shows the test setup. A specimen was placed at the center of a 3000 kN UTM for central axial compression loading. 4 LVDTs were set up at the corners of the end-plates of the specimen as shown in the Fig. 2. The axial displacement in load-axial displacement curves was obtained by averaging the values measured by the 4 LVDTs. Axial loads were applied by the UTM at a 0.001 mm/sec speed to observe failure procedures of specimens and local buckling.

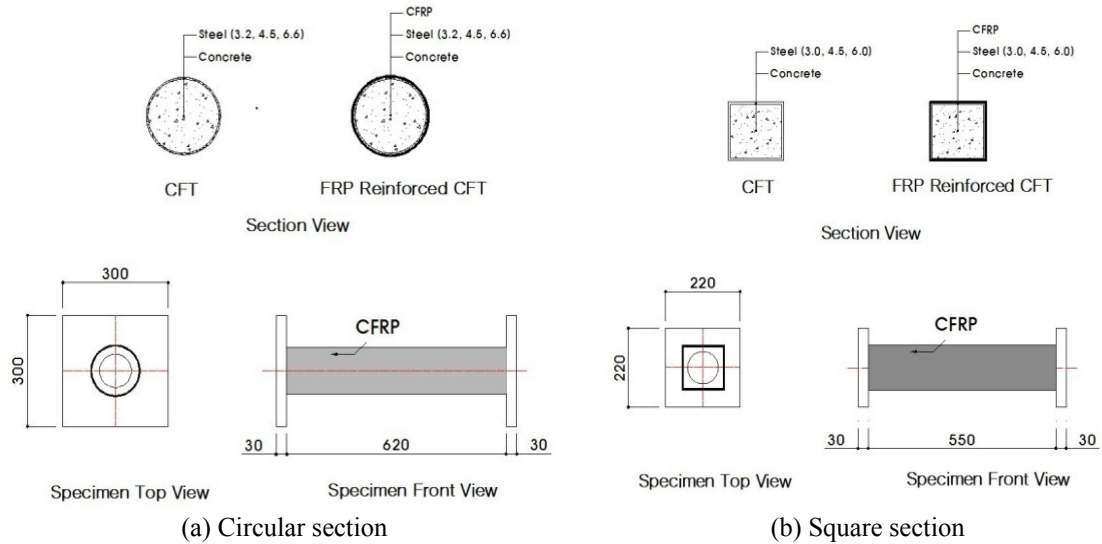


Fig. 1 Specimen details

Table 1 Plan for specimens and test parameters

Section types	Specimen	Size (mm)	D/t (B/t)	F_y (MPa)	CFS layers
Circular	C3N	D139.8 × 3.2	44	365	-
	C3F-1	D139.8 × 3.2	44	365	1
	C3F-3	D139.8 × 3.2	44	365	3
	C4N	D139.8 × 4.5	31	334	-
	C4F-1	D139.8 × 4.5	31	334	1
	C4F-2	D139.8 × 4.5	31	334	2
	C4F-3	D139.8 × 4.5	31	334	3
	C6N	D139.8 × 6.6	21	301	-
	C6F-1	D139.8 × 6.6	21	301	1
C6F-3	D139.8 × 6.6	21	301	3	
Square	R3N	125 × 125 × 3.0	39	304	-
	R3F-1	125 × 125 × 3.0	39	304	1
	R3F-3	125 × 125 × 3.0	39	304	3
	R4N	125 × 125 × 4.5	28	300	-
	R4F-1	125 × 125 × 4.5	28	300	1
	R4F-3	125 × 125 × 4.5	28	300	3
	R6N	125 × 125 × 6.0	21	324	-
	R6F-1	125 × 125 × 6.0	21	324	1
	R6F-3	125 × 125 × 6.0	21	324	3

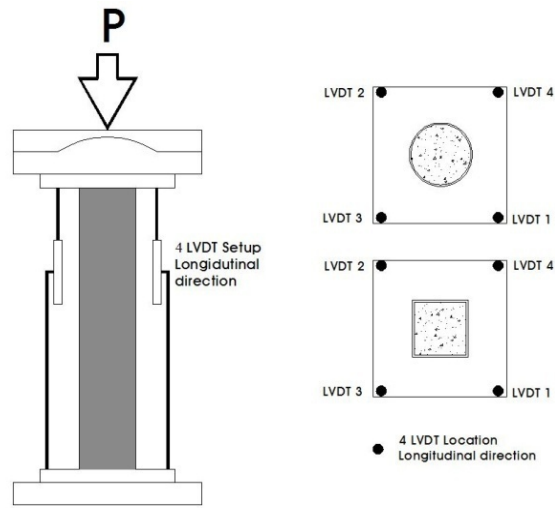


Fig. 2 Test setup



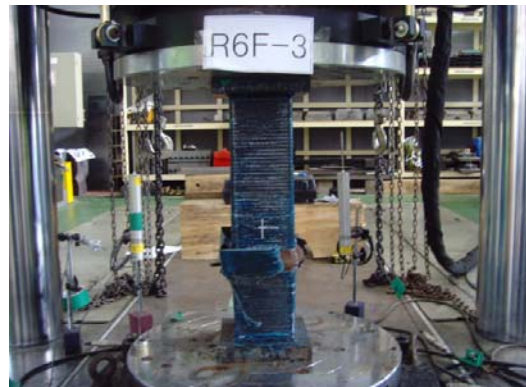
(a) FRP rupture
(C4F-1, Axial displacement = 7.1 mm)



(b) Final failure shape (C4F-1)



(c) FRP rupture
(R6F-3, Axial displacement = 10 mm)



(d) Final failure shape (R6F-3)

Fig. 3 Specimen failure procedure

2.4 Specimen failure procedure and load-displacement curve

Fig. 3 shows failure procedures of the specimens under different degrees of loading. Lateral expansion was observed on the entire body of circular specimens. As loading continued, lateral expansion of the specimens caused the rupture of CFRP. As shown in Fig. 3(b), rupture extended throughout the entire body of the column. (In C3F-3 specimen, CFRP rupture was observed at the lower part of the specimen.) Local buckling at the upper or lower parts of columns was followed by final failure.

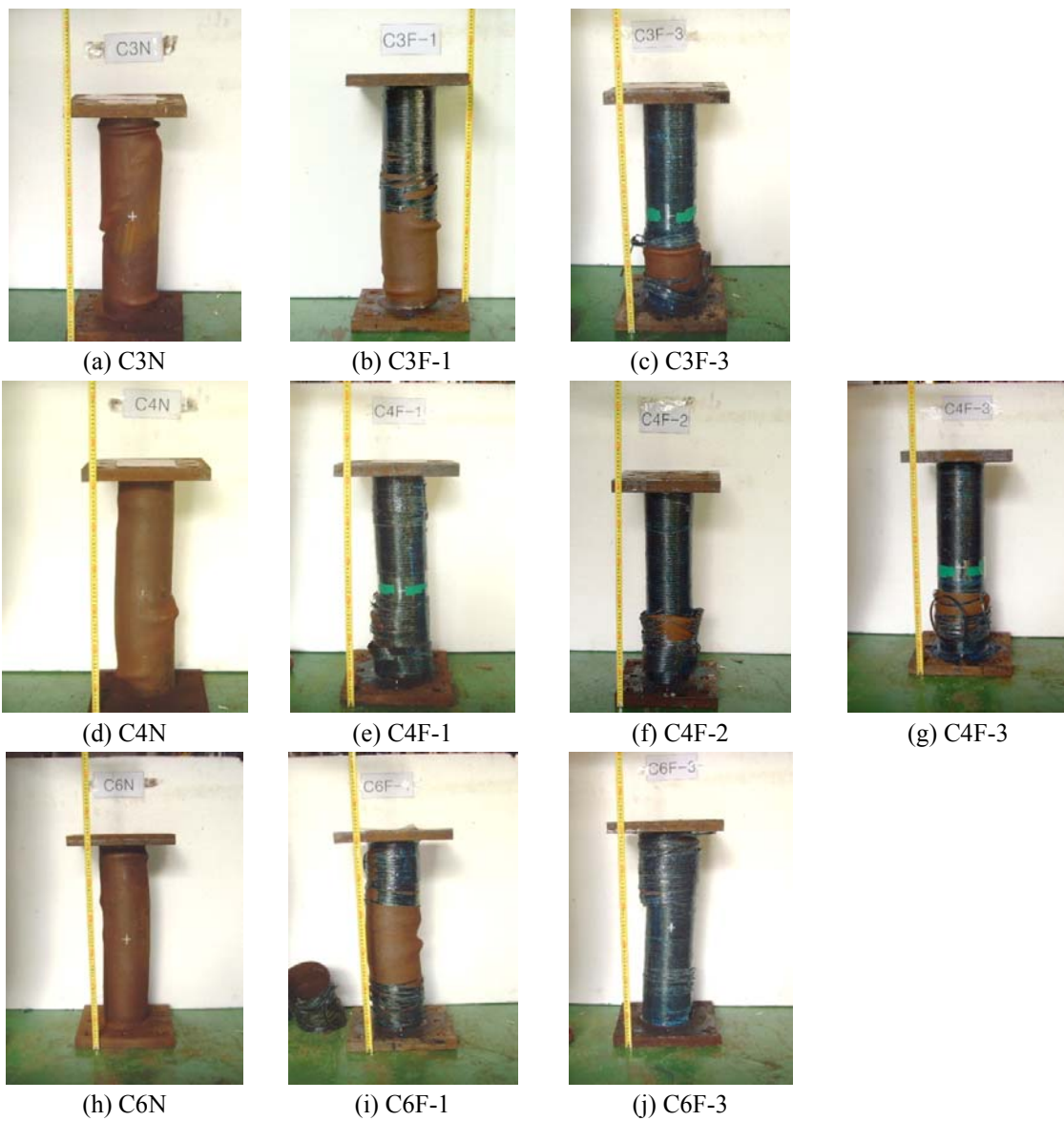


Fig. 4 Failure of circular specimens (Circular CFT)

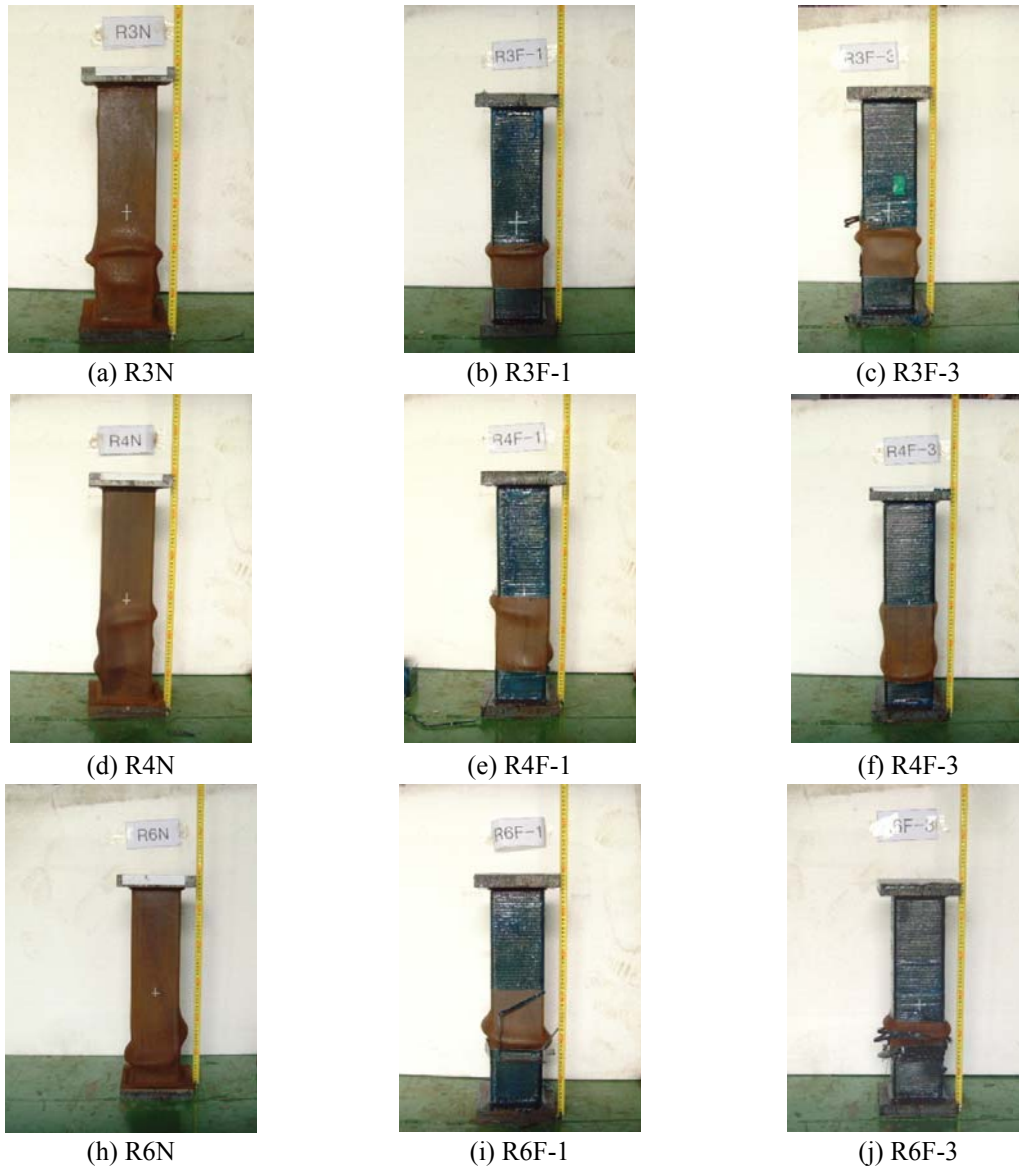


Fig. 5 Failure of square specimens (Square CFT)

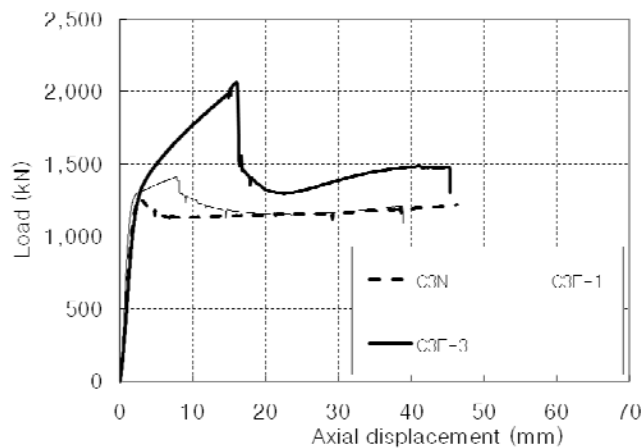
While no changes were observed in the square columns at the initial stage of loading, local buckling was observed at 15~25 cm from the lower ends of the columns as loading continued. CFRP sheets started to rupture as local buckling extended and the rupture zone of CFRP sheets also extended shown in Fig. 3(c). The steel tubes of columns were bent laterally, causing local buckling and finally failed.

Figs. 4 and 5 show the final failure shape of each specimen.

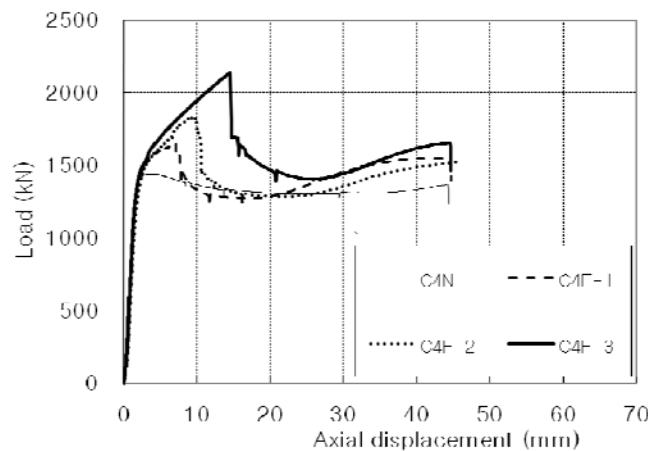
Fig. 6 shows the load-displacement curves of the specimens. Like unstrengthen square CFT columns, unstrengthen circular CFT columns showed linear behavior at the initial stage of loading

followed by the deterioration in load capacity. However, in CFRP strengthened circular CFT columns, maximum load capacity was enhanced and bi-linear behavior characterized by continuous enhancement of load capacity even after linear section was observed. Then, CFRP sheets ruptured at maximum load capacity followed by rapid deterioration in load capacity. However, C6F-1 specimen showed the behavior similar to that of strengthened specimens and C6F-3 showed a bit slighter degeneration in load capacity.

Unstrengthen square CFT columns presented load capacity deterioration after maximum load capacity and showed a constant load capacity curve after that. In CFT square columns strengthened with CFRP sheets, stair-shaped deterioration in load capacity was observed meaning the load capacity degenerated at each point when the CFRP sheets ruptured. In R6F-3 specimen, the rupture of CFRP sheets at the axial displacement of 10mm was immediately followed by rapid deterioration of load capacity and failure. Although the amount of the axial displacement where maximum load capacity was generated increased as the number of CFRP sheet layers increased,

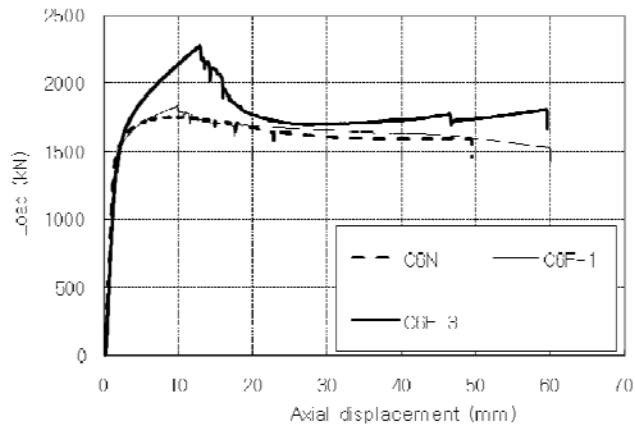


(a) Load-displacement curve (C3 specimen group)

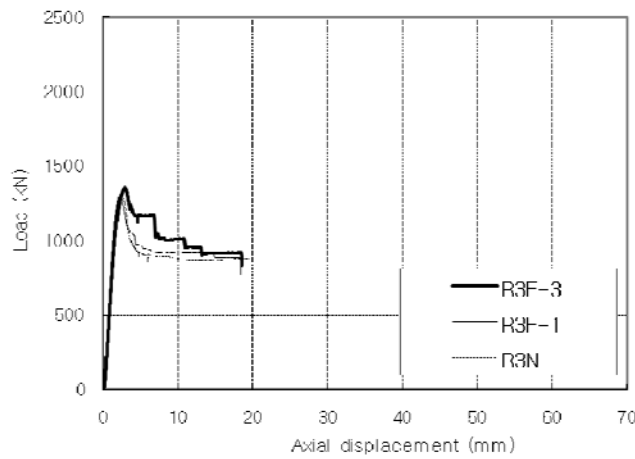


(b) Load-displacement curve (C4 specimen group)

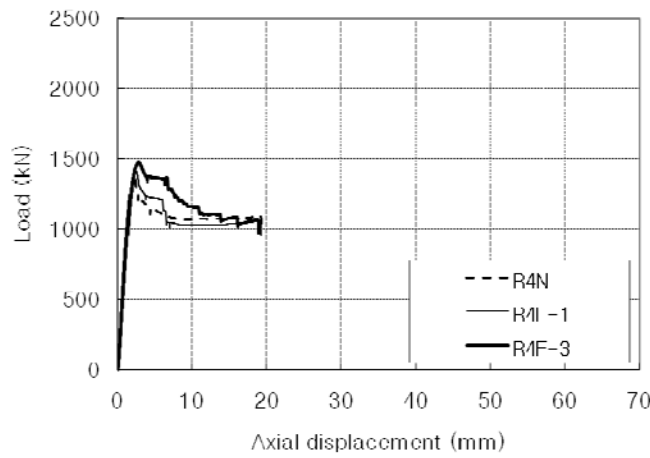
Fig. 6 Continued



(c) Load-displacement curve (C6 specimen group)

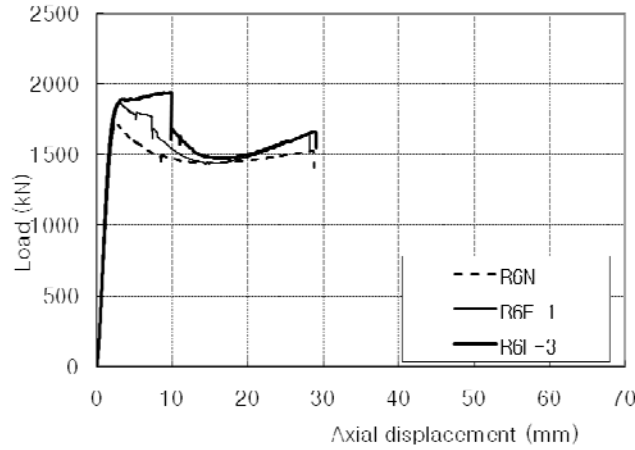


(d) Load-displacement curve (R3 specimen group)



(e) Load-displacement curve (R4 specimen group)

Fig. 6 Continued



(f) Load-displacement curve (R6 specimen group)

Fig. 6 Load-displacement curves

the amount of increase was nominal.

With regard to the specimens' behavior after yield point in association with sectional shape and width-thickness or diameter-thickness ratio, square specimens, in general, showed strain-softening behavior after yield point, while circular specimens showed strain-hardening behavior after yield point. However, both unstrengthened and strengthened specimens in R6 group which had relatively smaller width-thickness ratio of 21 showed strain-hardening behavior after yield. It was observed that sectional shape and width-thickness ratio exert an influence on the behavior of the specimens after yield point.

3. Test result review

3.1 Maximum load capacity

Table 2 shows the maximum load capacity of the specimens. In CFT square columns, although maximum load capacity improved as the number of CFRP sheet layers increased when compared with existing CFT square columns, the enhancement of load capacity associated with the number of layers was not significant. On the other hand, in CFT circular columns, the confinement effect enabled by the reinforcement with CFRP sheets whose tensile load capacity is ten times that of steel enhanced compressive load capacity of the concrete inside the columns and maximum load capacity of the specimens significantly when compared with existing CFT circular columns. Load capacity enhancement index (SEI) evaluation was conducted to observe the strengthening effect of CFRP sheets. SEI is defined as shown in Eq. (1) (Tao *et al.* 2007a). Table 2 shows the SEI values of specimens obtained from the test results.

$$SEI = \frac{P_{FRP,max} - P_{CFT,max}}{P_{CFT,max}} \quad (1)$$

Table 2 SEI evaluation (Effect of CFRP layers on SEI value)

Section types	Specimen	P_{\max} (kN)	SEI (Eq. (4)) (%)	
Circular	C3N	1252.4	-	
	C3F-1	1409.2	12.5	
	C3F-3	2062.9	64.6	
	C4N	1444.5	-	
	C4F-1	1653.3	14.5	
	C4F-2	1839.6	27.4	
	C4F-3	2139.3	48.1	
	C6N	1757.1	-	
	C6F-1	1833.6	4.33	
	C6F-3	2274.6	29.4	
	Square	R3N	1285.5	-
		R3F-1	1308.8	1.79
R3F-3		1357.0	5.60	
R4N		1372.2	-	
R4F-1		1409.3	2.70	
R4F-3		1473.5	7.36	
R6N		1727.3	-	
R6F-1		1866.4	8.05	
R6F-3		1936.3	12.1	

Where, $P_{CFT,\max}$ and $P_{FRP,\max}$ mean the maximum load capacity of unreinforced CFT columns and that of FRP-reinforced CFT columns, respectively.

The maximum SEI values for CFT circular and square columns were 64.6 and 12.1 obtained from C3F-3 and R6F-3, respectively. The increase in the number of CFRP sheet layers led to the slight increase of SEI in square CFT columns, while it enabled continuous increase of SEI in circular CFT columns. It is induced that the load capacity reinforcement effect provided by the CFRP sheets hardly enhances the load capacity of CFT square columns, whereas it improves that of CFT circular columns. This is due to the additional confinement effect of CFRP sheets.

In conclusion, in terms of maximum load capacity, the CFRP sheet retrofitting is more influential in CFT circular columns where the confinement effect enables the enhancement of load capacity than in CFT square columns.

3.2 Initial stiffness

In order to evaluate the initial stiffness of the specimens, Eq. (2) for initial stiffness was developed based on the displacement and load capacity at yield point calculated by the 1/3 tangent method. The concept of 1/3 tangent method is shown in the Fig. 7.

$$K_i = \frac{P_y}{\delta_y} \tag{2}$$

Where, δ_y and P_y mean the displacement and load strength at yield point, respectively. Fig. 8 shows the initial stiffness values of CFT circular and square specimens.

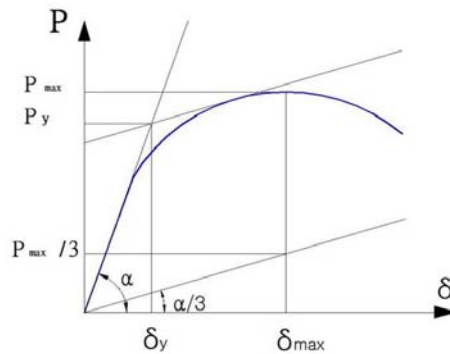
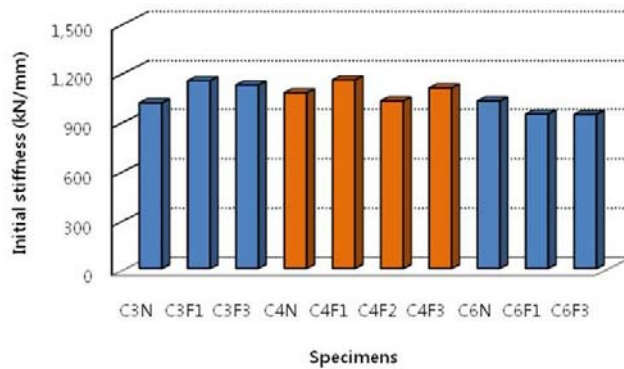
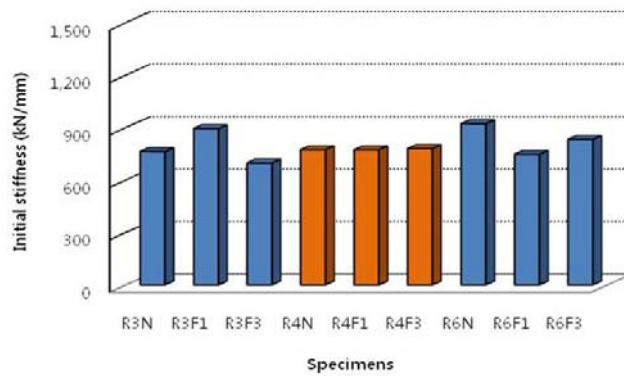


Fig. 7 Concept of 1/3 tangent method



(a) Initial stiffness of circular specimens



(b) Initial stiffness of square specimens

Fig. 8 Initial stiffness of specimens

As shown in Fig. 8, although slight differences in initial stiffness among the specimens were observed, it was almost constant regardless of the number of CFRP sheet layers. It is induced that CFRP strengthening enhances load capacity, while it does not exert a great influence on initial stiffness. It means that carbon fiber sheets do not enable strengthening effect until the yield point of the specimens. Actually, unstrengthened CFT specimens and CFRP strengthened CFT specimens presented almost identical load-displacement curves and yield points. That is why initial stiffness was almost identical among the specimens. And, the initial stiffness of circular specimens was higher than that of square specimens. It is induced that the enhancement of load capacity of CFT circular columns enabled by confinement effect leads to the improvement of the load capacity at yield point and thus the enhancement of initial stiffness.

3.3 Ductility

The ductility index of the specimens was defined as Eq. (3).

$$DI = \frac{\delta_u}{\delta_y} \quad (3)$$

In the formula, yield displacement (δ_y) was calculated by the 1/3 tangent method and the point of maximum load capacity was used as failure point (δ_u).

With ductility enhancement of 11%, 108% and 38% in the specimens which had B/t of 39, 28 and 21, respectively, Circular specimens also showed the ductility enhancement of 381%, 235% and 23% in the specimens which had D/t of 44, 31 and 21, respectively. Table 3 shows the ductility index of the specimens. CFT specimens showed the enhancement of ductility in association with the increase in the number of CFRP layers. This was due to the confinement of the CFRP sheet induced from the local buckling of steel tubes is slow.

3.4 Behavior comparison of circular and rectangular CFT

Fig. 9 shows the concept of confined concrete model for steel and CFRP sheet, respectively. The behavior of confined concrete model is differently shown for each of the confinement material.

For FRP confined concrete, the stress-strain curves of FRP confined concrete have bilinear behavior. At the low strain rate, the behavior of FRP confined concrete is similar to that of the unconfined concrete. With increasing strain rate, the stress of FRP confined concrete is linearly increased until the rupture point of FRP sheets, because FRP has a linear elastic stress-strain curve until FRP rupture point (Fig. 9(c)).

However, for steel confined concrete, the stress is decreased after peak stress point. Because, the steel has elasto-plastic stress-strain curve, the lateral confining pressure is constant after steel yielding point. Therefore, the stress deterioration can be shown for steel confined concrete (Fig. 9 (b)).

Similarly, for FRP strengthened circular CFT, it is shown that the load-displacement of each specimen curves has bi-linear behavior similarly to the FRP confined concrete. This is because the additional confinement effect by FRP sheets. When the CFT column is subjected to an axial compression load, the concrete expands and this expansion is confined by the steel tube. However, the lateral expansion of concrete catches up with the lateral expansion of the steel tube and the

Table 3 Ductility Index (DI) of specimens (Effect on CFRP layers on ductility)

Types	Specimen	DI (Ductility Index)	DI improvement
Circular	C3N	1.65	1.00
	C3F-1	4.52	2.20
	C3F-3	6.28	3.81
	C4N	3.28	1.00
	C4F-1	4.83	1.47
	C4F-2	5.73	1.75
	C4F-3	7.72	2.35
	C6N	6.17	1.00
	C6F-1	6.81	1.10
C6F-3	7.62	1.23	
Square	R3N	1.88	1.00
	R3F-1	1.89	1.01
	R3F-3	2.09	1.11
	R4N	1.94	1.00
	R4F-1	2.15	1.11
	R4F-3	4.03	2.08
	R6N	3.80	1.00
	R6F-1	4.31	1.05
	R6F-3	5.26	1.38

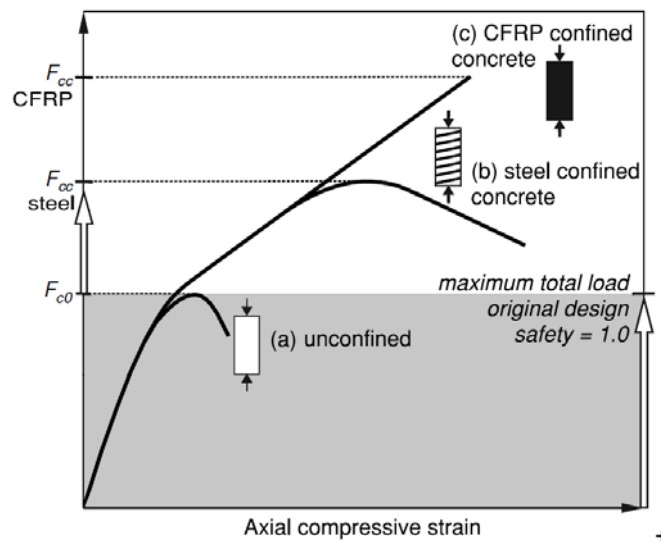


Fig. 9 The stress-strain curves of (a) unconfined concrete; (b) steel confined concrete, (c) FRP confined concrete

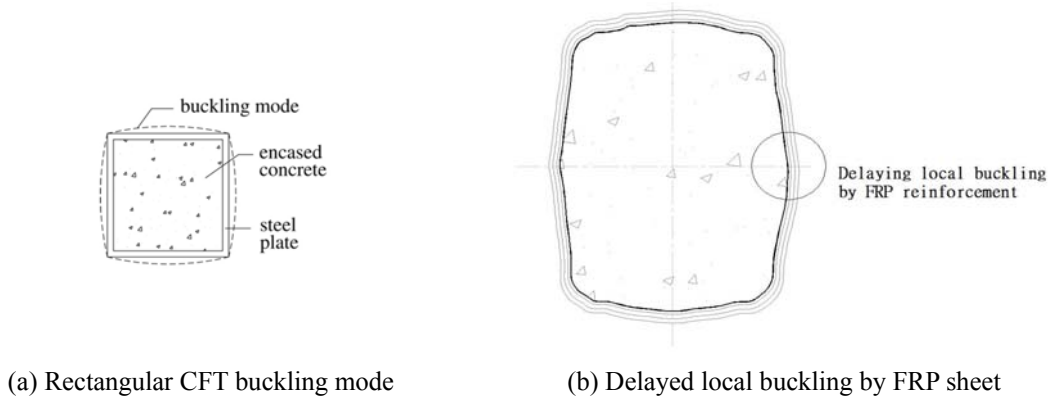


Fig. 10 The concept of delayed local buckling by FRP sheets

lateral expansion is confined by the steel tube. With the intensified loading, the steel tube will laterally expand and FRP confinement is activated. From the failure behavior of circular specimens, the load-displacement curve of FRP strengthened circular CFT columns is similar to that of the current columns in the first linear stage. In the second linear stage, FRP confinement is activated and the load linearly increases because FRP has a linear elastic stress-strain curve.

However, square steel tubes can provide little confinement of the concrete because the wall of the square tube resisted the concrete pressure by plate bending, instead of the hoop stresses. As a result, infilled concrete strength is slightly increased. The buckling mode is shown in Fig. 10(a). The buckling occurred toward outside of the steel tube. From Fig. 10(b), it is shown that the FRP sheet can delay local buckling of the steel tubes. Therefore, slight load improvement can be shown with increasing the number of FRP sheet layer because of delayed local buckling of steel tube.

4. Ultimate load capacity prediction

Since the CFRP confinement has no significant effect on ultimate capacity of rectangular CFT columns in this test, calculation method is discussed only for CFRP strengthened circular CFT columns. Two methods will be presented and the predicted values will be compared with this study's test results and other researcher's test results (Gu *et al.* 2004, Xiao *et al.* 2005, Tao *et al.* 2007).

4.1 ACI 440 code applied method

ACI Committee 440 (2002) has taken an approach that is equivalent to the Mander, Priestley, Park equation (1988) for the ultimate strength of confined concrete. This equation can be applied to not only steel tube confined concrete but also FRP confined concrete.

$$f'_{cc} = f'_{co} \left[2.25 \sqrt{1 + 7.9 \frac{f_l}{f'_{co}}} - 2 \frac{f_l}{f'_{co}} - 1.25 \right] \quad (4)$$

Where, f'_{cc} , f'_{co} and f_l mean compressive strength of confined concrete, compressive strength of unconfined concrete and lateral confinement pressure of confined concrete.

Because CFRP strengthened circular CFT is confined by steel tube and CFRP sheet, the lateral confinement pressure can be expressed as Eq. (5) also, d means diameter of core concrete.

$$f_l = \frac{2f_s t_s}{d} + \frac{2f_{FRP} t_{FRP}}{d} \quad (5)$$

Therefore, based on the Mander's equation, the following formula is proposed in this paper.

$$P_u = A_s F_y + A_c f'_{cc} \quad (6)$$

4.2 Simplified confined concrete model method

Several of the existing strength models (Samaan *et al.* 1998, Karbhari *et al.* 1997, Saffi *et al.* 1999) for Steel or FRP confined concrete take the following form.

$$\frac{f'_{cc}}{f'_{co}} = 1 + k_1 \frac{f_l}{f'_{co}} \quad (7)$$

Where, f'_{cc} , f'_{co} and f_l mean compressive strength of confined concrete, compressive strength of unconfined concrete and lateral confinement pressure of confined concrete, respectively, and k_1 is the confinement effectiveness coefficients. To obtain the k_1 value for steel tubes and CFRP sheets confined concrete, 23 data were used for evaluating the axial compressive strength of steel-CFRP confined concrete (Xiao *et al.* 2005, Tao *et al.* 2007). From the test data, the following equation for the axial compressive strength of steel-CFRP confined concrete is proposed for predicting

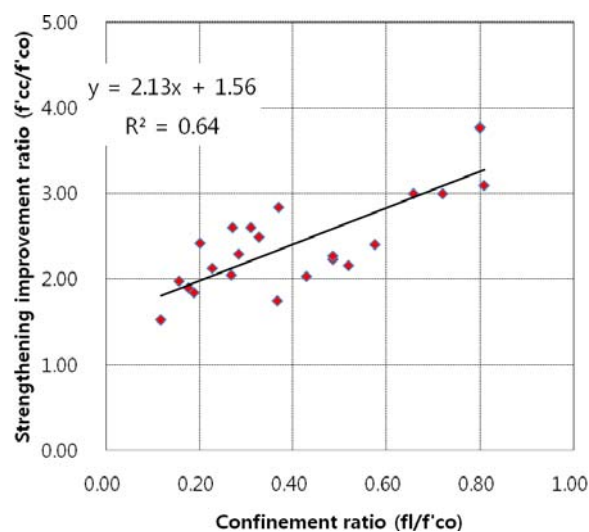


Fig. 11 Trends of strength data of steel-CFRP confined concrete

Table 4 Comparisons of experimental and predicted ultimate strengths for specimens

Specimen label	d (mm)	f'_{co} (MPa)	t_s (mm)	t_{FRP} (mm)	Layer of CFRP	f_y (MPa)	f_{FRP} (MPa)	P_{ue} (kN)	P_{uc} / P_{ue} (Eq. (6))	P_{uc} / P_{ue} (Eq. (6))
Gu <i>et al.</i> (2004)										
1-1.5	124	36.85	1.5	0.167	1	350	1260	1085.8	0.93	0.97
1-2.5	124	36.85	2.5	0.167	1	350	1260	1293.6	0.98	0.97
1-3.5	124	36.85	3.5	0.167	1	310	1260	1347.5	1.05	1.03
1-4.5	124	36.85	4.5	0.167	1	310	1260	1689.3	0.97	0.94
2-1.5	124	36.85	1.5	0.167	2	350	1260	1282.8	0.85	0.85
2-2.5	124	36.85	2.5	0.167	2	350	1260	1506.3	0.88	0.86
2-3.5	124	36.85	3.5	0.167	2	310	1260	1592.5	0.92	0.89
2-4.5	124	36.85	4.5	0.167	2	310	1260	1846.3	0.91	0.88
Xiao <i>et al.</i> (2005)										
CCFT2L-1	146.1	46.6	2.95	1.4	2	356	897	2230	1.18	1.13
CCFT2L-2	146.1	46.6	2.95	1.4	2	356	897	2266	1.16	1.11
CCFT4L-1	146.1	46.6	2.95	1.4	4	356	897	3439	0.88	0.88
CCFT4L-2	146.1	46.6	2.95	1.4	4	356	897	3438	0.88	0.88
Tao <i>et al.</i> (2007)										
C1-1	150	47.8	3	0.17	1	230	4212	3316.6	1.04	1.05
C1-2	150	47.8	3	0.17	2	230	4212	3316.6	0.98	0.95
C2-1	244	47.8	3	0.17	1	230	4212	5354.4	1.07	1.16
C2-2	244	47.8	3	0.17	2	230	4212	5354.4	0.99	1.02
Park (this study)										
C3F-1	133.4	37.5	3.2	0.111	1	358	3500	1409.2	1.27	1.22
C3F-3	133.4	37.5	3.2	0.111	3	358	3500	2062.9	1.01	0.99
C4F-1	130.8	37.5	4.5	0.111	1	328	3500	1653.3	1.18	1.13
C4F-2	130.8	37.5	4.5	0.111	2	328	3500	1839.6	1.14	1.10
C4F-3	130.8	37.5	4.5	0.111	3	328	3500	2139.3	1.03	1.02
C6F-1	126.6	37.5	6.6	0.111	1	295	3500	1833.6	1.17	1.13
C6F-3	126.6	37.5	6.6	0.111	3	295	3500	2274.6	1.04	1.04

ultimate strength of CFRP strength circular CFT

$$\frac{f'_{cc}}{f'_{co}} = 1.56 + 2.13 \frac{f_l}{f'_{co}} \quad (8)$$

Where, the lateral confinement pressure can be expressed as Eq. (9)

$$f_l = \frac{2f_s t_s}{d} + \frac{2f_{FRP} t_{FRP}}{d} \quad (9)$$

Fig. 11 shows a trends of strength data of steel-CFRP confined concrete. Therefore, based on the simple model, the following formula is proposed in this paper.

$$P_u = A_s F_y + A_c f'_{cc} \quad (9)$$

4.3 Comparison of experimental and predicted ultimate strengths for specimens

The predicted ultimate loads (P_{uc}) using Eqs. (6) and (9) are compared with the experimental values (P_{ue}) obtained in this paper and other paper (Gu *et al.* 2004, Xiao *et al.* 2005, Tao *et al.* 2007). The comparison is shown in Table 4.

The mean values is 1.02 for first method (Mander's equation) and 1.01 for second method (Simplified confined concrete model), respectively. As can be seen, the prediction values are good agreement with the test results obtained in this study and in the literature.

5. Conclusions

In this study, axial load tests for CFRP strengthened CFT square and circular columns were conducted and their failure behavior was compared with that of existing unstrengthen CFT square and circular columns. Their failure behavior, compressive load capacity, initial stiffness, ductility and the influence of FRP-reinforcement were compared. The following is the conclusion obtained from the study.

1. For CFRP strengthened CFT square columns, the load capacity of the columns deteriorated gradually presenting stair-shaped curves after maximum load capacity point on load-axial displacement relationship which showed that load capacity degenerated at each point when the CFRP sheets ruptured. However, CFT circular columns showed continuous increase in load capacity after yield point thanks to the confinement effect enabled by CFRP sheets and double linear behavior on load-axial displacement curves. After that, load capacity deteriorated rapidly upon the rupture of the CFRP sheets.
2. The load capacity of CFT square columns was enhanced by approximately 19% as the number of CFRP sheet layers increased. However, in CFT circular columns, load capacity was enhanced by approximately 67% proving the influence of the CFRP sheets reinforcement. Therefore, CFRP retrofitting can enhance the load capacity of the circular CFT column effectively, whereas the enhancement is not significant for square CFT columns.
3. The initial stiffness of the specimens was almost identical regardless of layers of CFRP sheets. However, the ductility of CFRP strengthened CFT circular and square columns increased with increasing number of CFRP layers because of delaying the local buckling of steel tubes by CFRP sheets.
4. Simple formulas are proposed for predicting the ultimate load capacity for CFRP strengthened circular CFT columns. In general, the prediction values are in good agreement with the test values.

Acknowledgements

This research was supported by the Ministry of Knowledge Economy by the Korea government (No. 20111 020100040).

References

- AISC (2005), Steel Construction Manual, 2, (13th Edition), American Institute of Steel Construction.
- ACI 440R-96 (2002), Guide for the Design and Construction of Externally Bonded FRP Systems for Strengthening Concrete Structures, ACI Committee 440.
- Bambach, M.R., Jema, H.H. and Elchalakani, M. (2009), "Axial capacity and design of thin-walled steel SHS strengthened with CFRP", *Thin-Walled. Struct.*, **47**(1), 1112-1121.
- El-Tawil, S., Ekiz, E., Goel, S. and Chao, S.H. (2011), "Restraining local and global buckling behavior of steel plastic hinges CFRP", *J. Construct. Steel. Res.*, **67**(1), 261-269.
- Fam, A., Macfougall, C. and Shaat, A. (2009), "Upgrading steel-concrete composite girders and repair of damaged steel Beams using bonded CFRP laminates", *Thin-Walled. Struct.*, **47**(1), 1122-1135
- Gu, W. Guan, C.W. Zhao, Y.H. and Cao. H. (2004), "Experimental study on concentrically-compressed circular concrete filled CFRP -steel composite tubular short columns", *J. Shenyang Architect. Civil Eng. Univ.*, **20**(2), 118-120.
- Harries, K.A. Peck, A.J. and Abraham, E.J. (2009), "Enhancing stability of structural steel sections using FRP", *Thin-Walled. Struct.*, **47**(1), 1092-1101.
- Karbhari, V.M. and Gao, Y. (1997), "Composite jacketed concrete under uniaxial compression-verification of simple design equation", *ASCE, J. Mater. in Civil Eng.*, **19**(4), 185-193.
- Mander, J.B. Priestley, M.J. and Park, R. (1988), "Theoretical stress-strain model for confined concrete", *ASCE, J. Struct. Eng.*, **114**(8), 1084-1826.
- Miller, T.C., Chajes, M.J., Mertz, D.R. and Hastings, J.N. (2001), "Strengthening of a steel bridge girder using CFRP plates", *ASCE, J. Bridge. Eng.*, **6**(6), 514-522.
- Narmashiri, K., Jumaat, M.Z. and Ramil Sulong, N.H. (2010), "Shear strengthening of steel I-beams by using CFRP strips", *Scientific Research and Essays.*, **5**(16), 2155-2168.
- Park, J.W., Hong, Y.K. and Choi, S.M. (2010), "Behavior of concrete filled square tubes confined by carbon fiber sheets (CFS) under compression and cyclic Loads", *Steel Compos. Struct., Int. J.*, **8**(2), 187-205.
- Sallam, H.E.M., Badawy, A.A.M., Saba, A.M. and Mikhail, F.A. (2010), "Flexural behavior of strengthened steel-concrete composite beams by various plating methods", *J. Const. Steel. Res.*, **62**(1), 472-483.
- Saffi, M., Toutanji, H.A. and Li, Z. (1999), "Behaviors of concrete columns confined with fiber reinforced Polymer tubes", *ACI Materials Journal.*, **96**(4), 500-509.
- Samaan, M., Mirmiran, A. and Shaawy, M. (1998), "Model of concrete confined by fiber composites", *ASCE, J. Struct. Eng.*, **124**(9), 1025-1031.
- Schneider, S.P. (1998), "Axially loaded concrete-filled steel tubes", *ASCE, J. Struct. Eng.*, **121**(10), 1125-1138.
- Schnerch, D., Danwood. M., Rizkalla. S. and Sumner, E. (2007), "Proposed design guidelines for strengthening of steel bridges with FRP Materials", *Const. Build. Mater.*, **21**(5), 1001-1010.
- Schnerch, D. and Rizkalla. S. (2008), "Flexural strengthening of steel bridges with high modulus CFRP strips", *ASCE, J. Bridge. Eng.*, **13**(2), 192-201.
- Shaat, A. and Fam, A.Z. (2009), "Slender steel columns strengthened using high-modulus CFRP plates for buckling control", *ASCE, J. Compo. Const.*, **13**(1), 1-12.
- Tao, Z., Han, L.H. and Wang, L.L. (2007a), "Axial loading behaviors of CFRP strengthened concrete-filled steel tubular stub columns", *Adv. Struct. Eng.*, **10**(1), 37-46.
- Tao, Z., Han, L.H. and Wang, L.L. (2007b), "Compressive and flexural behavior of CFRP-repaired concrete-filled steel tubes after exposure to fire", *J. Cons. Steel. Res.*, **63**(8), 1116-1126.

- Teng, J.G. and Hu, Y.M. (2007), "Behavior of FRP-jacked circular steel tubes and cylindrical shells under axial compression", *Const. Build. Mater.*, **21**(3), 827-838.
- Xiao, Y., He, W. and Choi, K.K. (2005), "Confined concrete-filled tubular columns", *ASCE, J. Struct. Eng.*, **131**(3), 488-497.

CC